

ACCEPTED VERSION

Simarpreet Kaur, Cheryl Suwen Law, Nathan Hu Williamson, Ivan Kempson, Amirali Popat, Tushar Kumeria and Abel Santos

Environmental copper sensor based on polyethylenimine-functionalized nanoporous anodic alumina interferometers

Analytical Chemistry, 2019; 91(8):5011-5020

This document is the Accepted Manuscript version of a Published Work that appeared in final form in Analytical Chemistry, copyright © 2019 American Chemical Society after peer review and technical editing by the publisher. To access the final edited and published work see <http://dx.doi.org/10.1021/acs.analchem.8b04963>

PERMISSIONS

<http://pubs.acs.org/page/4authors/jpa/index.html>

The new agreement specifically addresses what authors can do with different versions of their manuscript – e.g. use in theses and collections, teaching and training, conference presentations, sharing with colleagues, and posting on websites and repositories. The terms under which these uses can occur are clearly identified to prevent misunderstandings that could jeopardize final publication of a manuscript (**Section II, Permitted Uses by Authors**).

[Easy Reference User Guide](#)

7. Posting Accepted and Published Works on Websites and Repositories: A digital file of the Accepted Work and/or the Published Work may be made publicly available on websites or repositories (e.g. the Author's personal website, preprint servers, university networks or primary employer's institutional websites, third party institutional or subject-based repositories, and conference websites that feature presentations by the Author(s) based on the Accepted and/or the Published Work) under the following conditions:

- It is mandated by the Author(s)' funding agency, primary employer, or, in the case of Author(s) employed in academia, university administration.
- If the mandated public availability of the Accepted Manuscript is sooner than 12 months after online publication of the Published Work, a waiver from the relevant institutional policy should be sought. If a waiver cannot be obtained, the Author(s) may sponsor the immediate availability of the final Published Work through participation in the ACS AuthorChoice program—for information about this program see <http://pubs.acs.org/page/policy/authorchoice/index.html>.
- If the mandated public availability of the Accepted Manuscript is not sooner than 12 months after online publication of the Published Work, the Accepted Manuscript may be posted to the mandated website or repository. The following notice should be included at the time of posting, or the posting amended as appropriate:
"This document is the Accepted Manuscript version of a Published Work that appeared in final form in [JournalTitle], copyright © American Chemical Society after peer review and technical editing by the publisher. To access the final edited and published work see [insert ACS Articles on Request author-directed link to Published Work, see <http://pubs.acs.org/page/policy/articlesonrequest/index.html>]."
• The posting must be for non-commercial purposes and not violate the ACS' "Ethical Guidelines to Publication of Chemical Research" (see <http://pubs.acs.org/ethics>).
- Regardless of any mandated public availability date of a digital file of the final Published Work, Author(s) may make this file available only via the ACS AuthorChoice Program. For more information, see <http://pubs.acs.org/page/policy/authorchoice/index.html>.

18 June 2020

<http://hdl.handle.net/2440/119226>

Environmental Copper Sensor Based on Polyethyleneimine-Functionalized Nanoporous Anodic Alumina Interferometers

Simarpreet Kaur, Cheryl Suwen Law, Nathan Hu Williamson, Ivan M Kempson, Amirali Popat, Tushar Kumeria, and Abel Santos

Anal. Chem., **Just Accepted Manuscript** • DOI: 10.1021/acs.analchem.8b04963 • Publication Date (Web): 22 Feb 2019

Downloaded from <http://pubs.acs.org> on February 23, 2019

Just Accepted

“Just Accepted” manuscripts have been peer-reviewed and accepted for publication. They are posted online prior to technical editing, formatting for publication and author proofing. The American Chemical Society provides “Just Accepted” as a service to the research community to expedite the dissemination of scientific material as soon as possible after acceptance. “Just Accepted” manuscripts appear in full in PDF format accompanied by an HTML abstract. “Just Accepted” manuscripts have been fully peer reviewed, but should not be considered the official version of record. They are citable by the Digital Object Identifier (DOI®). “Just Accepted” is an optional service offered to authors. Therefore, the “Just Accepted” Web site may not include all articles that will be published in the journal. After a manuscript is technically edited and formatted, it will be removed from the “Just Accepted” Web site and published as an ASAP article. Note that technical editing may introduce minor changes to the manuscript text and/or graphics which could affect content, and all legal disclaimers and ethical guidelines that apply to the journal pertain. ACS cannot be held responsible for errors or consequences arising from the use of information contained in these “Just Accepted” manuscripts.



Environmental Copper Sensor Based on Polyethyleneimine-Functionalized Nanoporous Anodic Alumina Interferometers

Simarpreet Kaur¹, Cheryl Suwen Law^{2,3,4}, Nathan Hu Williamson^{1,5}, Ivan Kempson^{1*}, Amirali Popat⁶, Tushar Kumeria^{6*} and Abel Santos^{2,3,4*}

¹*Future Industries Institute, University of South Australia, Mawson Lakes, South Australia 5095, Australia.*

²*School of Chemical Engineering, The University of Adelaide, South Australia 5005, Australia.*

³*Institute for Photonics and Advanced Sensing, The University of Adelaide, South Australia 5005, Australia.*

⁴*ARC Centre of Excellence for Nanoscale BioPhotonics, The University of Adelaide, South Australia 5005, Australia.*

⁵*Eunice Kennedy Shriver National Institute of Child Health and Human Development, National Institutes of Health, Bethesda, Maryland, USA.*

⁶*School of Pharmacy, The University of Queensland, PACE Building, Queensland 4012, Australia.*

*E-mails: ivan.kempson@unisa.edu.au ; t.kumeria@uq.edu.au ; abel.santos@adelaide.edu.au

ABSTRACT

Anthropogenic copper pollution of environmental waters from sources such as acid mine drainage, antifouling paints and industrial waste discharge is a major threat to our environment and human health. This study presents an optical sensing system that combines self-assembled glutaraldehyde-crosslinked double-layered polyethyleneimine (PEI-GA-PEI)-modified nanoporous anodic alumina (NAA) interferometers with reflectometric interference spectroscopy (RIfS) for label-free, selective monitoring of ionic copper in environmental waters. Calibration of the sensing system with analytical solutions of copper shows a linear working range between 1 and 100 mg L⁻¹, and a low limit of detection of 0.007 ± 0.001 mg L⁻¹ (i.e. ~0.007 ppm). Changes in the effective optical thickness (ΔOT_{eff}) of PEI-GA-PEI-functionalized NAA interferometers are monitored in real-time by RIfS, and correlated with the amount of ionic copper present in aqueous solutions. The system performance is validated through X-ray photoelectron spectroscopy (XPS) and the spatial distribution of copper within the nanoporous films is characterized by time-of-flight secondary ion mass spectroscopy (ToF-SIMS). The specificity and chemical selectivity of the PEI-GA-PEI-NAA sensor to Cu²⁺ ions is verified by screening six different metal ion solutions containing potentially interfering ions such as Al³⁺, Cd²⁺, Fe³⁺, Pb²⁺, Ni²⁺ and Zn²⁺. Finally, the performance of the PEI-GA-PEI-NAA sensor for real-life applications is demonstrated using legacy acid mine drainage liquid and tap water for qualitative and quantitative detection of copper ions. This study provides new opportunities to develop portable, cost-competitive and ultra-sensitive sensing systems for real-life environmental applications.

Keywords: Copper, Chelation, Nanoporous Anodic Alumina, Polyethyleneimine, Reflectometric Interference Spectroscopy

INTRODUCTION

The use of copper is constantly increasing in materials and products of commercial importance such as cosmeceuticals,¹ agriculture,² construction,³ chemical industries,⁴ and electronics^{3,5}. This rapid diversification and expansion in the use of copper is dramatically increasing its impact on natural environments. Copper can be released into the environment during its mining and also from copper-based products such as metal-based biocides in agriculture, antifouling paints in marine systems^{6,7}, and domestic and industrial waste emissions⁸⁻¹⁰. Once released into the environment, copper becomes highly soluble and percolates into soil and water in its various toxic forms.^{11,12} Copper is a broad spectrum biocide, being free ionic (Cu^{2+}) and inorganic complexes ($\text{Cu}(\text{OH})^+$) its most toxic forms.¹³ The maximum permissible limit of Cu^{2+} ions in drinking water cannot exceed 2 mg L^{-1} (i.e. 2 ppm) and 1.3 mg L^{-1} (i.e. 1.3 ppm), as established by the World Health Organization (WHO) and the US Environmental Protection Agency (EPA), respectively.¹⁴ Therefore, there is an urgent need to develop monitoring systems that can perform highly sensitive, selective, cost-competitive, user-friendly and reliable detection of copper ions in environmental waters. Current benchmark techniques used to detect copper in aqueous solutions include inductively coupled plasma optical emission spectroscopy/mass spectroscopy (ICP-OES/MS),¹⁵ atomic absorption spectroscopy (AAS),¹⁶ anodic stripping voltammetry (ASV),¹⁷ UV-Visible¹⁸ and fluorescence spectroscopy¹⁹. Though these methods offer good detection limits and broad linear working ranges, they require significant capital and maintenance investments, laborious sample preparation processes and highly trained personnel, and cannot be miniaturized into portable sensing systems for in-situ analysis applications.

Current progress in nanotechnology is enabling development of advanced analytical tools for heavy metal ions sensing. An outstanding example of this is the combination of thin

1
2
3 nanoporous films with optical techniques such as fluid imbibition-coupled laser interferometry²⁰,
4 interferogram average over wavelength²¹ and reflectometric interference spectroscopy (RIfS)²²⁻²⁸.
5
6 These systems provide novel approaches for developing label-free optical sensors able to monitor
7
8 binding events in real-time. The nanoporous structure of sensing platforms such as porous silicon
9
10 and nanoporous anodic alumina (NAA) enables enhanced sensitivities due to their high surface
11
12 area, which provides more ligand sites for binding interactions. Chemical functionalization of
13
14 these nanoporous substrates enables high chemical selectivity toward a broad range of analyte
15
16 species such as proteins,²⁹ small molecules³⁰ and ions³¹ nucleotides^{32,33} and whole cells^{34,35}.

21
22 This study presents an innovative optical sensing system combining chemically modified
23
24 NAA optical interferometers with RIfS for sensitive and highly selective detection of copper ions
25
26 (**Figures 1a and b**). The novelty stems from our identification that the modification of the surface
27
28 chemistry of NAA interferometers with layers of glutaraldehyde crosslinked polyethyleneimine
29
30 (PEI-GA-PEI) gives this system chemical selectivity to specifically detect copper ions in aqueous
31
32 solutions. The interaction between copper ions and PEI-GA-PEI-modified NAA interferometers
33
34 is translated into quantifiable changes in the effective optical thickness of these nanoporous films
35
36 (i.e. sensing principle) (**Figures 1c and d**). PEI-GA-PEI chemical functional layers provide
37
38 excellent selectivity toward copper ions in complex real-life environmental solutions containing
39
40 interfering organic and inorganic impurities (**Figures 1e and f**).³⁶⁻³⁸ The performance of this
41
42 copper sensing system is systematically assessed in terms of working range, sensitivity, linearity,
43
44 low limit of detection, chemical selectivity and real-life application. Our study provides new
45
46 opportunities to develop ultra-sensitive, highly selective, low-cost, portable sensing systems able
47
48 to monitor trace levels of copper ions in environmental waters.
49
50
51
52
53
54
55
56
57
58
59
60

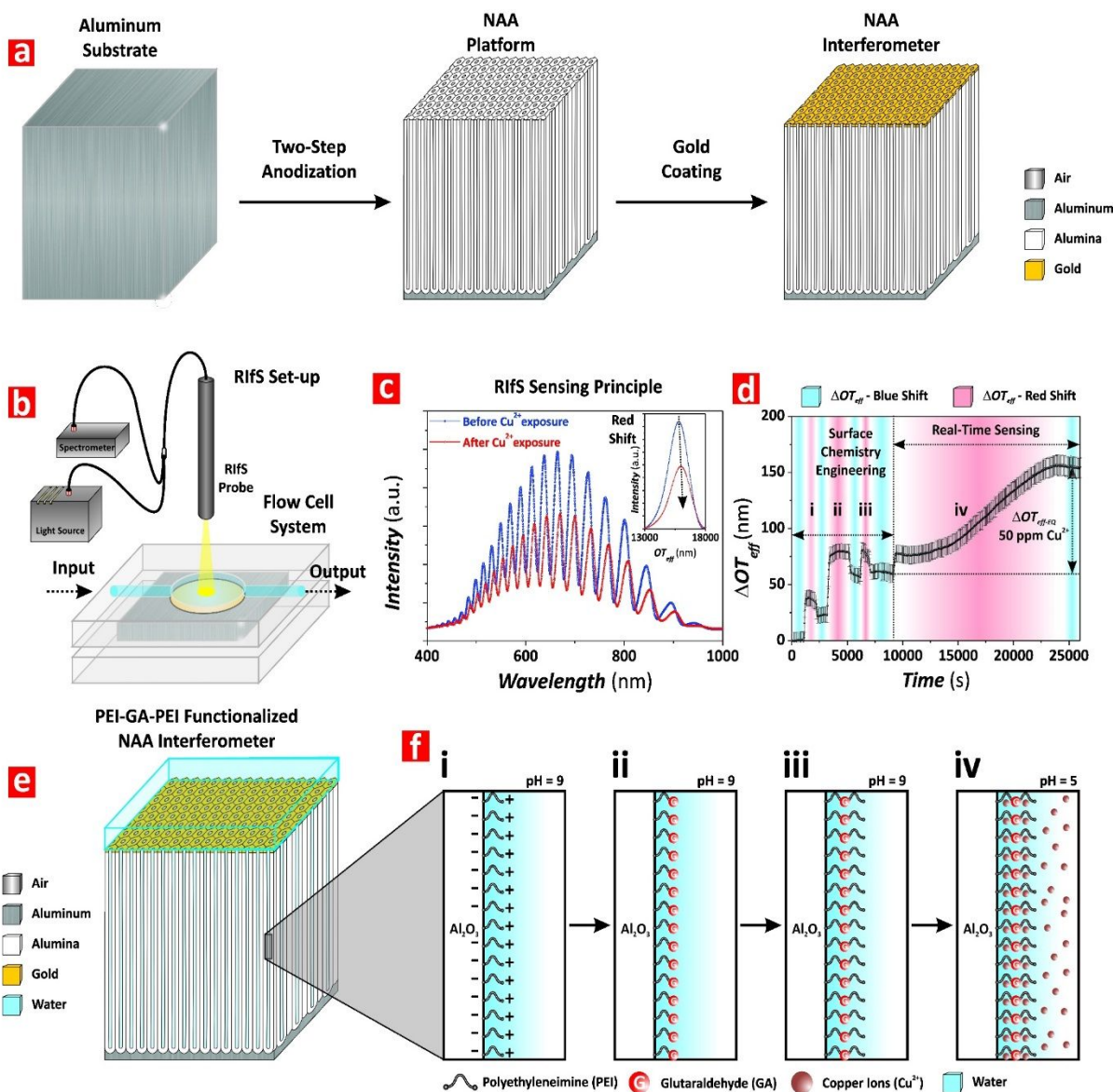


Figure 1. Production of PEI-GA-PEI-functionalized NAA interferometers and assessment of binding affinity for detection of copper ions using RIFS. a) Illustration describing the two-step anodization process used to produce NAA interferometers (left – aluminum substrate; center – NAA interferometer; right – gold-coated NAA interferometer). b) Schematic showing the RIFS set-up used to monitor binding interactions between PEI-GA-PEI-modified NAA interferometers and copper ions in real-time under dynamic flow conditions. c) Representative RIFS spectra of PEI-GA-PEI-functionalized NAA interferometers before and after exposure to Cu^{2+} ions (inset showing the characteristic fast Fourier transform (FFT) spectra used to estimate the effective optical thickness (OT_{eff}) of NAA interferometers associated with the different stages of the process: surface chemistry engineering (i–iii) and real-time sensing (iv)). d) Real-time effective optical thickness changes (ΔOT_{eff}) associated with the surface chemistry engineering and sensing stages: (i) electrostatic functionalization of the inner surface of the nanopores of NAA interferometers with PEI molecules; (ii) crosslinking of immobilized PEI molecules with glutaraldehyde (GA); (iii) immobilization of second PEI functional layer; and (iv) binding to Cu^{2+}

ions. e) Schematic showing the structure of PEI-GA-PEI-functionalized NAA interferometers. f) Illustration showing details of the inner surface chemistry of gold-coated PEI-GA-PEI-functionalized NAA interferometers during the different stages of the sensing process (i–iv).

EXPERIMENTAL SECTION

2.1. Materials. High purity (99.9997 %) aluminum (Al) foils of thickness 0.32 mm were purchased from Goodfellow Cambridge Ltd (UK). Oxalic acid ($\text{H}_2\text{C}_2\text{O}_4$), perchloric acid (HClO_4), chromic acid (H_2CrO_4), lead(II) nitrate ($\text{Pb}(\text{NO}_3)_2$), nickel(II) sulfate (NiSO_4), zinc chloride (ZnCl_2), aluminum chloride hexahydrate ($\text{AlCl}_3 \cdot 6\text{H}_2\text{O}$), cadmium nitrate tetrahydrate ($\text{Cd}(\text{NO}_3)_2 \cdot 4\text{H}_2\text{O}$), iron chloride (FeCl_3), hydrochloric acid (HCl), nitric acid (HNO_3) and glutaraldehyde (GA) were acquired from Sigma-Aldrich (Australia). Ethanol ($\text{C}_2\text{H}_5\text{OH}$), phosphoric acid (H_3PO_4), sodium chloride (NaCl) and copper (II) sulphate pentahydrate ($\text{CuSO}_4 \cdot 5\text{H}_2\text{O}$) were purchased from ChemSupply (Australia). Branched polyethyleneimines (PEI) Lupasol® G20 (50 wt % in H_2O , MW 1300 g mol^{-1}), Lupasol® HF (56 wt % in H_2O , MW 25000 g mol^{-1}), and Lupasol® P (50 wt % in H_2O , MW 750000 g mol^{-1}) were provided by BASF (Germany) and stored under N_2 till use. Real legacy acid mine drainage solution was kindly provided by Copper Mines of Tasmania (Australia). Ultrapure water 18.2 $\text{M}\Omega \text{ cm}$ from a Milli-Q® Advantage A10® water purification system was used to prepare all the aqueous solutions used in this study. pH adjustments were performed using an ION 700 meter (Eutech instruments, Singapore).

2.2 Fabrication of NAA Interferometers. Al substrates were sonicated in EtOH and ultrapure water for 15 min each and dried under air stream. Then Al chips were electropolished in a mixture of HClO_4 and EtOH 1:4 (v:v) at 20 V and 5 °C for 3 min in an electrochemical reactor with a circular window of ~1 cm in diameter. The first anodization step was performed in 0.3 M oxalic acid electrolyte at 40 V and 6 °C for 20 h. The resulting NAA layer was chemically removed by wet etching in 0.2 M H_2CrO_4 and 0.4 M H_3PO_4 at 70 °C for 3 h. The second anodization step was

performed using the same conditions than those used during the first step but for 2 h. Finally, the NAA films were pore-widened by wet chemical etching in H₃PO₄ 5 wt % at 35 °C for 15 min.³⁹⁻⁴²

2.3. Optical Characterization. Details of the flow system and RIfS setup used in this study are provided in the **Supporting Information**. RIfS spectra (**Figures 1b-d**) were acquired in the wavelength range 400–1000 nm and processed by applying fast Fourier transform (FFT) to estimate the effective optical thickness (OT_{eff}) of NAA interferometers according to **Equation 1**:

$$OT_{eff} = 2n_{eff}L_p \cos \theta \quad (1) \text{ where}$$

OT_{eff} , n_{eff} and L_p are the effective optical thickness, the effective refractive index and the physical thickness of the NAA platform, respectively, whereas θ is the angle of incidence of light (i.e. $\theta = 0^\circ$ in this case).

2.4. Chemical Modification of NAA Interferometers. As-prepared NAA interferometers were coated with an ultrathin film of gold ~4-5 nm thick using a sputter coater equipped with film thickness monitor (sputter coater 108 Auto, Cressington, USA) to enhance the intensity of spectral fringes.⁴³⁻⁴⁵ Prior to sensing, the inner surface of NAA interferometers was chemically functionalized with GA-crosslinked double PEI layers through a three-step procedure monitored in real-time by RIfS. This process was performed in a flow cell system (**Supporting Information**) using effective optical thickness changes (ΔOT_{eff}) as sensing parameter. A stable baseline in water was obtained. Then, NAA interferometers were exposed to a PEI functional solution (0.2 wt %, 0.1 mol L⁻¹ NaCl, pH 9) till complete saturation of the inner surface by PEI functional groups, denoted by a plateau in (ΔOT_{eff}) (**Figure 1d-i**). Milli-Q water was injected into the system to remove loosely bound PEI molecules from the inner surface of NAA interferometers. Self-assembled PEI molecules immobilized onto the inner surface of the NAA interferometers by electrostatic interaction were crosslinked by exposing the nanoporous films to 2.5 v % GA solution

1
2
3 for a given time, followed by a thorough washing with Milli-Q water (**Figure 1d-ii**). The sensing
4 platforms were then exposed to fresh PEI functional solution (0.2 wt %, 0.1 mol L⁻¹ NaCl, pH 9)
5
6 as in the first step to crosslink a secondary layer of PEI molecules (**Figure 1d-iii**). Finally, Milli-
7
8 Q water was flowed through the system to remove unbounded PEI molecules .
9
10

11
12 **2.5. Calibration and Detection of Cu²⁺ Ions.** After functionalization (sections i–iii, **Figure 1d**),
13 the sensing performance of PEI-GA-PEI-modified NAA interferometers was assessed by
14 measuring ΔOT_{eff} upon exposure to six different concentrations of Cu²⁺, ranging from 1 to 100 mg
15 L⁻¹ at pH 5. These copper analytical solutions were prepared by diluting 0.1 M stock solution of
16 Cu₂SO₄·5H₂O in Milli-Q water. PEI-GA-PEI-modified NAA interferometers were packed in a
17 flow cell system, through which the copper analytical solutions were flowed at an optimized rate
18 of 100 μL min⁻¹ using a peristaltic pump (LongerPump®, Thermoline Scientific, Australia). A
19 stable baseline was first established in Milli-Q water at pH 5 for ~15 min before injection of ionic
20 copper solutions into the flow cell. Binding of copper ions to PEI-GA-PEI-functionalized NAA
21 interferometers was monitored in real-time through changes in ΔOT_{eff} by RIFS. This process
22 continued until all the available ligand sites in the inner surface of NAA were saturated with Cu²⁺
23 ions. Control experiments were performed with non-functionalized NAA interferometers using 10
24 and 100 mg L⁻¹ analytical solutions of Cu²⁺.
25
26
27
28
29
30
31
32
33
34
35
36
37
38
39
40
41

42 **2.6. Assessment of Chemical Selectivity.** The chemical selectivity of the system toward copper
43 ions was assessed by exposing a set of freshly prepared PEI-GA-PEI-modified NAA sensing
44 platforms to 25 mg L⁻¹ individual aqueous solutions of Cd²⁺, Ni²⁺, Fe³⁺, Al³⁺, Pb²⁺ and Zn²⁺ ions.
45 Effective optical thickness changes upon exposure to these analytical solutions were compared
46 against those obtained for copper ions for the same concentration.
47
48
49
50
51
52
53
54
55
56
57
58
59
60

1
2
3 **2.7. Real-Life Environmental Application.** The performance of PEI-GA-PEI-modified NAA
4 interferometers to detect copper ions in complex matrices was evaluated using AMD and tap water
5 solutions with known Cu^{2+} concentration and benchmarked against ICP-OES. 100 mL of acid mine
6 drainage (AMD) liquid was poured into a 250 mL glass beaker and the pH was adjusted to 5 (i.e.
7 initial pH \sim 2.2). A 50 mL aliquot of supernatant containing dissolved metal ions was separated
8 from the precipitate and used for detection of copper content through RfS in PEI-GA-PEI-
9 modified NAA interferometers. The ion metal content of the AMD solution was established by
10 inductively coupled plasma optical emission spectroscopy (ICP-OES). Duplicates of the diluted
11 samples were acidified with 3–4 drops of HNO_3 to prevent bacterial growth. All the results were
12 processed with Multicomponent Spectral Fitting. Calibration standards and QC standards were
13 prepared in 1 % HNO_3 .
14
15
16
17
18
19
20
21
22
23
24
25
26
27

28 **2.8. Structural Characterization of NAA.** The structural features of the NAA interferometers
29 were established by field emission gun scanning electron microscopy (FEG-SEM FEI Quanta
30 450). FEG-SEM images were processed using ImageJ.
31
32
33
34
35

36 RESULTS AND DISCUSSION

37
38 **3.1. Structural Characterization of NAA Interferometers.** The geometric features of NAA
39 interferometers (i.e. nanopore diameter – d_p ; nanopore length – L_p ; and interpore distance – d_{int} ;
40 **Figure 2a**) were established by FEG-SEM image analysis. **Figures 2b–d** compile a set of
41 representative FEG-SEM images showing the cross-sectional (**Figures 2b and c**) and top (**Figure**
42 **2d**) views of NAA interferometers fabricated by two-step anodization process.³⁹⁻⁴² **Figure 2b**
43 shows a cross-sectional FEG-SEM image of a NAA interferometer featuring straight cylindrical
44 nanopores from top to bottom, which grow perpendicularly to the underlying aluminum substrate
45 during anodization. These nanopores have a closed oxide barrier layer at the bottom (**Figure 2c**),
46
47
48
49
50
51
52
53
54
55
56
57
58
59
60

with an average nanopore length of $L_p = 5.5 \pm 0.2 \mu\text{m}$ (i.e. physical thickness of the optical film). The top surface of NAA shows an array of nanopores of uniform size and distribution arranged in a self-organized hexagonal pattern (**Figure 2d**). The average nanopore diameter was $d_p = 65 \pm 4 \text{ nm}$, with an average interpore distance of $d_{int} = 105 \pm 5 \text{ nm}$. NAA interferometers with these geometric features display well-resolved and intense Fabry-Pérot interference fringes in their RfS spectra that are suitable for sensing applications.

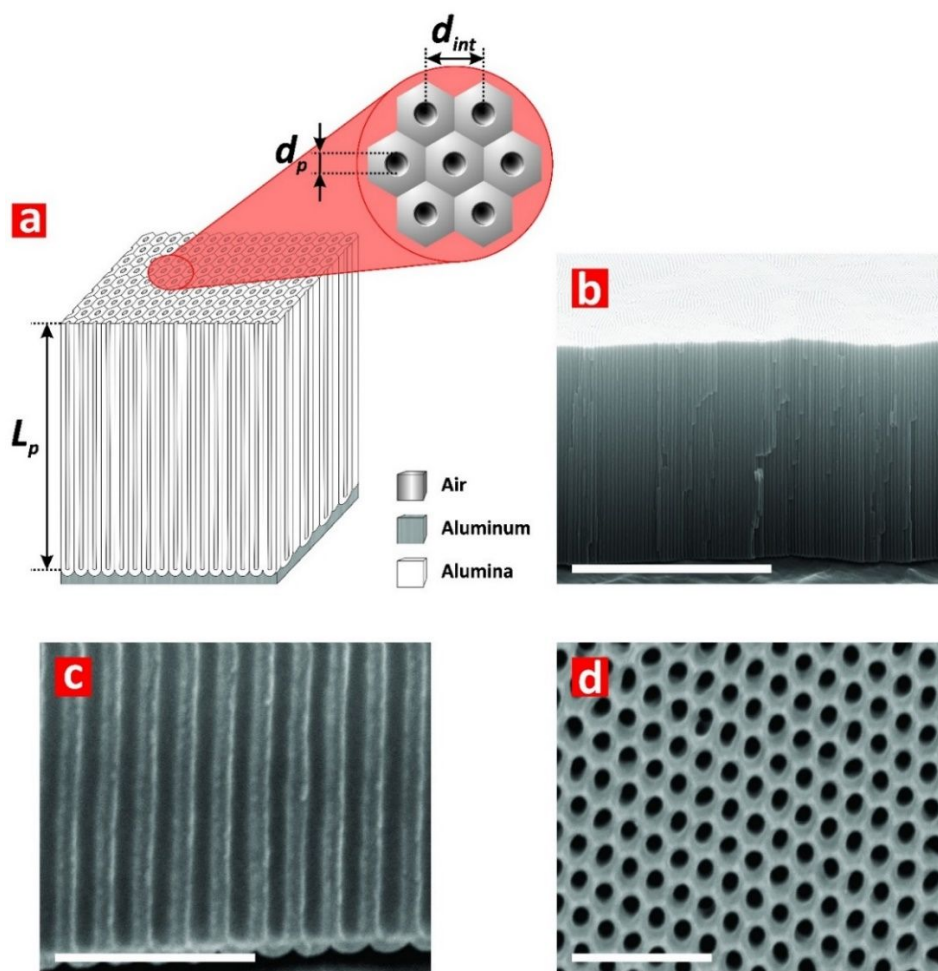


Figure 2. Structural features of NAA interferometers produced by two-step anodization. a) Schematic of a NAA interferometer with details of geometric features (i.e. nanopore diameter – d_p ; nanopore length – L_p ; and interpore distance – d_{int}). b) General cross-sectional FEG-SEM image view of a NAA interferometer featuring straight cylindrical nanopores from top to bottom (scale bar = $5 \mu\text{m}$). c) Magnified cross-sectional FEG-SEM image view

1
2
3 showing details of the oxide barrier layer (scale bar = 500 nm). d) Top FEG-SEM view of hexagonally arranged
4 cylindrical nanopores in NAA interferometers (scale bar = 500 nm).
5

6 **3.2. Preliminary Optimization of Sensing Features of NAA Interferometers.** Preliminary

7
8 experiments were carried out to optimize the sensing performance of PEI-GA-PEI-functionalized
9
10 NAA interferometers toward copper ions. Three sensing features were optimized: i) molecular
11
12 weight of PEI functional molecules, ii) flow rate of the analytical solutions, and iii) the surface
13
14 chemistry architecture of PEI-GA-PEI functional layers. These three parameters were selected for
15
16 their effect on the sensing performance of this system, as demonstrated in previous studies.^{46,47}
17
18

19
20 Freshly prepared PEI-GA-PEI-modified NAA interferometers were exposed to a 100 mg L⁻¹ Cu²⁺
21
22 analytical solution at pH 5. Effective optical thickness changes (ΔOT_{eff}) in these NAA sensing
23
24 platforms upon modification of these three working parameters were measured by RIfS to establish
25
26 the most optimal conditions for Cu²⁺ sensing. The obtained results, described in detail in the
27
28 **Supporting Information** and summarized in **Figure 3**, established that the best performing
29
30 combination of these working parameters was PEI molecules of 750000 g mol⁻¹ molecular weight
31
32 (**Figure 3a**), a flow rate of 100 μ L min⁻¹ (**Figure 3b**), and a sandwiched PEI-GA-PEI surface
33
34 chemistry architecture (**Figure 3c**).
35
36
37
38
39

40 **3.3. Real-Time Monitoring of Copper Ions.** The surface chemistry engineering and real-time

41
42 sensing (sections i–iii and iv in **Figure 1d**, respectively) were monitored in real-time by RIfS.
43
44 First, a ΔOT_{eff} baseline is established in Milli-Q water and 0.1 M NaCl in Milli-Q water at pH 9
45
46 for ~15 min each. No significant change in ΔOT_{eff} is observed during the transition from Milli-Q
47
48 water to NaCl solution. After this step, 0.2 wt % PEI solution in 0.1 M NaCl at pH 9 is injected
49
50 into the flow system. The exposure of the NAA interferometers to the PEI solution leads to a sharp
51
52 and rapid increase in ΔOT_{eff} , which stabilizes at a value of ~35 nm. The surface alumina (i.e. Al₂O₃)
53
54
55
56
57
58
59
60

is negatively charged at slightly basic pH (i.e. pH = 9). As a result, positively charged PEI molecules are immobilized onto the inner surface of alumina by strong electrostatic interactions.^{48,49} The adsorption of the PEI functional layer onto the inner surface of the nanopores increases the effective refractive index of the NAA interferometers, red-shifting the OT_{eff} of the optical film (**Figure 1d-i**).

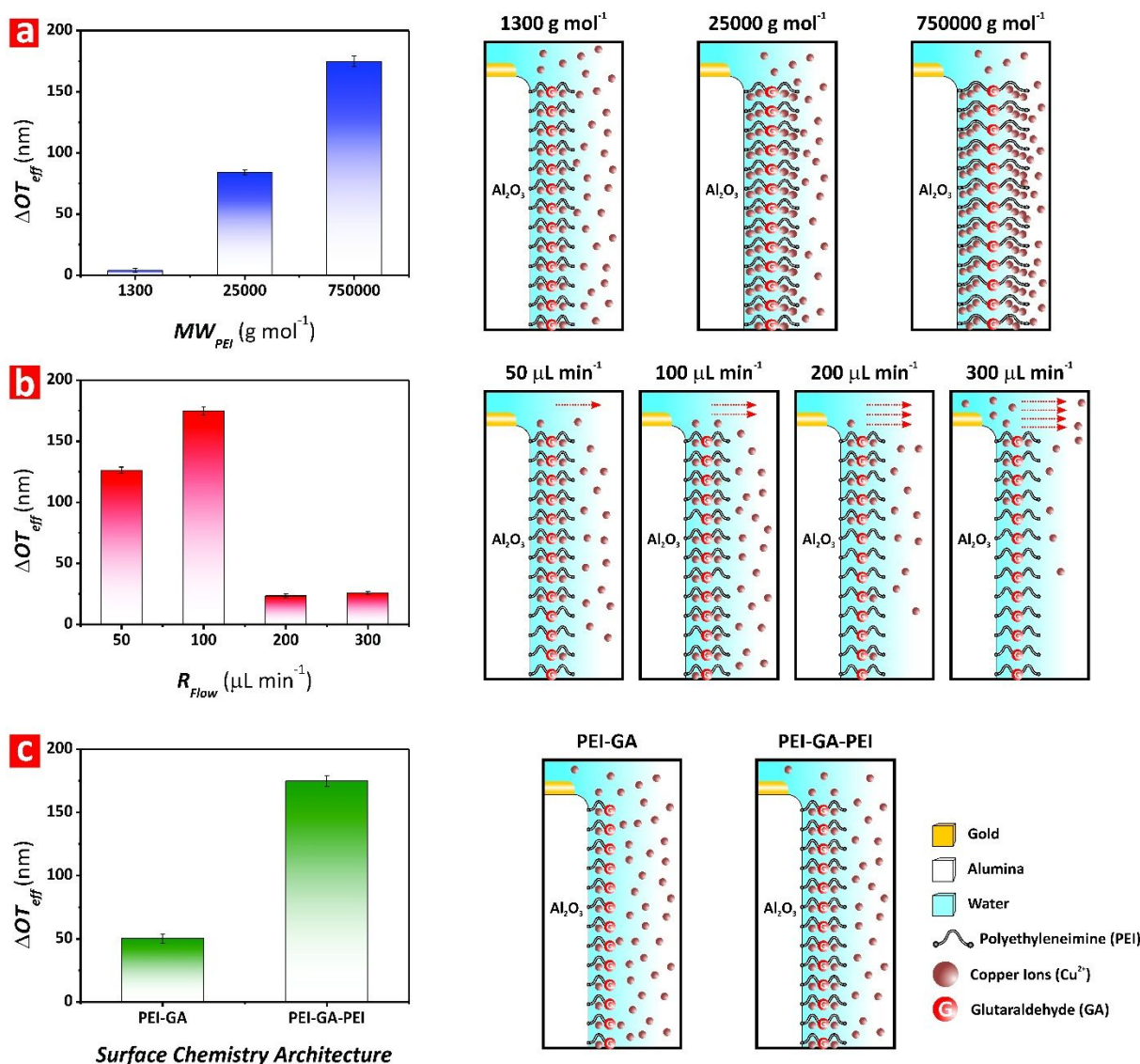


Figure 3. Optimization of working parameters to maximize sensing of Cu^{2+} ions in NAA interferometers (note: error bars denote standard deviation from average measurements obtained from $n = 3$ independent experiments). a) Bar chart showing the ΔOT_{eff} associated with each molecular weight of PEI assessed in this study (i.e. $MW_{PEI} =$

1
2
3 1300, 25000 and 750000 g mol⁻¹) (left) and illustration showing the effect of this working parameter on the sensing
4 performance of PEI-GA-PEI-modified NAA interferometers (right). b) Bar chart showing the ΔOT_{eff} associated
5 with each flow rate of analytical solution assessed in this study (i.e. $R_{flow} = 50, 100, 200$ and $300 \mu\text{L min}^{-1}$) (left)
6 and schematic showing the effect of this working parameter on the sensing performance of PEI-GA-PEI-modified
7 NAA interferometers (right). c) Bar chart showing the ΔOT_{eff} associated with each surface chemistry architecture
8 assessed in this study (i.e. PEI-GA and PEI-GA-PEI) (left) and illustration depicting the effect of this working
9 parameter on the sensing performance of PEI-GA-PEI-modified NAA interferometers (right).
10
11
12

13 After achieving a plateau (i.e. saturation of the inner surface of NAA with PEI molecules), fresh
14 0.1 M NaCl solution at pH 9 and Milli-Q water are sequentially flowed through the system. ΔOT_{eff}
15 slightly decreases to a new equilibrium value of ~ 23 nm during this stage, confirming a stable
16 adsorption of PEI functional layers. This slight blue shift in ΔOT_{eff} is collectively attributable to
17 lower refractive index of water and removal of loosely bound PEI molecules from the inner surface
18 of NAA. Next, PEI-modified NAA interferometers are exposed to a 2.5 v % GA solution in Milli-Q
19 water, resulting in a red shift in ΔOT_{eff} of ~ 79 nm (**Figure 1d-ii**). The chemical crosslinking of PEI
20 with GA enhances the stability of the PEI functional layer by creating intra-molecular bonds
21 between PEI molecules immobilized onto the inner surface of NAA. Once stabilized, Milli-Q
22 water and 0.1 M NaCl at pH 9 solutions are flowed through the system in a sequential fashion to
23 remove physisorbed GA molecules and to establish a new ΔOT_{eff} baseline prior to creating the
24 second PEI functional layer. During this process, ΔOT_{eff} blue-shifts and achieves a new stable
25 baseline at ~ 58 nm. Fresh PEI solution (0.2 wt %, 0.1 mol L⁻¹ NaCl, pH 9) is flowed again through
26 the system to create a double PEI functional layer crosslinked to the primary PEI layer through
27 GA (i.e. PEI-GA-PEI surface chemistry architecture) (**Figure 1d-iii**). Finally, 0.1 M NaCl at pH 9
28 and Milli-Q water solutions are sequentially flowed through the system. A total increment of ~ 4
29 nm in ΔOT_{eff} is observed after deposition of the second PEI functional layer, with the final
30 equilibrium baseline of ΔOT_{eff} achieved at ~ 62 nm. Then, PEI-GA-PEI-modified NAA
31 interferometers were exposed to different analytical solutions of Cu²⁺ ions with controlled
32
33
34
35
36
37
38
39
40
41
42
43
44
45
46
47
48
49
50
51
52
53
54
55
56
57
58
59
60

1
2
3 concentrations (i.e. real-time sensing stage – **Figure 1d-iv**). **Figure 4a** shows a representative
4
5 example of real-time monitoring of ΔOT_{eff} upon exposure to $[Cu^{2+}] = 75$ ppm solution (**Figure S1**
6
7 in the Supporting Information summarizes the obtained result for all the Cu^{2+} ions concentrations).
8
9
10 As this graph reveals, ΔOT_{eff} increases sharply upon exposure to the analytical solution containing
11
12 Cu^{2+} until the binding groups present in the PEI functional layers are completely saturated with
13
14 Cu^{2+} ions (i.e. plateau in ΔOT_{eff}). The chemical binding between Cu^{2+} ions and the functional
15
16 groups of GA-crosslinked PEI layers red-shifts the RfS interference pattern. For instance, as
17
18 **Figure 4a** shows, when PEI-GA-PEI-modified NAA platforms are exposed to a 75 mg L^{-1} solution
19
20 of Cu^{2+} ions, ΔOT_{eff} increases progressively up to ~ 130 nm, from the previously established
21
22 baseline in Milli-Q water, until it achieves a stable value. This indicates that the PEI functional
23
24 layers inside the nanopores of NAA are saturated with Cu^{2+} ions (i.e equilibrium state). Once the
25
26 binding equilibrium state is achieved, Milli-Q water at pH 5 is flowed through the system to
27
28 remove unbound Cu^{2+} ions and to establish the total ΔOT_{eff} associated with 75 mg L^{-1} of Cu^{2+} ions,
29
30 which was measured to be ~ 124 nm with respect to the previous baseline obtained in Milli-Q
31
32 water. The kinetics of this binding reaction for each $[Cu^{2+}]$ is also characterized by the saturation
33
34 time (t_{sat}), defined as the time at which the equilibrium state is reached, as indicated in **Figure 4a**.
35
36 **Figure 4b** summarizes the average ΔOT_{eff} values for each surface chemistry engineering stage (i.e.
37
38 first PEI functional layer, GA crosslinking, and second PEI functional layer) and real-time sensing
39
40 (i.e. for $[Cu^{2+}] = 1$ to 100 ppm).

41
42
43 **3.4. Calibration of PEI-GA-PEI-Modified NAA Interferometers for Cu^{2+} Sensing.** The
44
45 sensing performance of our RfS system was assessed by flowing analytical solutions of Cu^{2+} ions
46
47 with controlled concentrations, from 1 to 100 mg L^{-1} . The sensing parameters characterizing the
48
49 performance of this system (i.e. linear working range, sensitivity, saturation time and low limit of
50
51
52
53
54
55
56
57
58
59
60

1
2
3 detection) were estimated by correlating ΔOT_{eff} and t_{sat} values for each Cu^{2+} ions concentration, as
4 summarized in **Figure 4c**. This graph shows a strong linear correlation between ΔOT_{eff} and $[Cu^{2+}]$
5
6 for the entire range of concentrations (1–100 mg L⁻¹). A linear fitting between these parameters
7
8 establishes the sensitivity (i.e. slope (S) = 1.55 ± 0.11 nm (mg L⁻¹)⁻¹) and the low limit of detection
9
10 (i.e. $LoD = 0.007 \pm 0.001$ mg L⁻¹), calculated as the slope of the fitting line and $3\sigma = 3$ times the
11
12 standard deviation of the lowest concentration of copper ions divided by the slope of the fitting
13
14 line, respectively, with a linear working range from 1 to 100 mg L⁻¹ and a linearity of $R^2 = 0.9926$.
15
16 As **Figure 4c** shows, t_{sat} is relatively constant for $[Cu^{2+}] < 75$ ppm. However, the saturation time
17
18 increases above $[Cu^{2+}] = 75$ ppm and decreases moderately for $[Cu^{2+}] = 100$ ppm, with an average
19
20 $t_{sat} = 4.7 \pm 1.5$ h, and $t_{sat-max} = 7.3$ h and $t_{sat-min} = 3.1$ h. The response time achieved by PEI-GA-
21
22 PEI-functionalized NAA interferometers under the conditions of study is comparable to that
23
24 reported in previous studies using NAA interferometers of similar nanoporous geometry and
25
26 dynamic flow conditions.^{27,32,46,48,50} The main factor establishing the kinetics of copper ions is the
27
28 binding mechanism to PEI-GA-PEI functional layers. PEI is a polymer with a branched structure
29
30 and high content of amine-nitrogen functional groups with repeating C_2H_5N units that donate
31
32 electrons and chelate metal ions.⁵¹ Nitrogen atoms in PEI chelate Cu^{2+} ions by coordination
33
34 interaction, in which four nitrogen atoms bind one Cu^{2+} ion. The branched structure of the PEI-
35
36 GA-PEI functional layer prevents the direct exposure of all the functional groups in the PEI
37
38 molecules immobilized onto the inner surface of NAA interferometers. The progressive binding
39
40 of copper ions leads to conformational changes in PEI molecules so four nitrogen atoms can
41
42 chelate one Cu^{2+} ion. These conformational changes expose more functional binding sites in the
43
44 PEI molecules, creating new binding interactions with Cu^{2+} ions and a progressive increment of
45
46 ΔOT_{eff} .
47
48
49
50
51
52
53
54
55
56
57
58
59
60

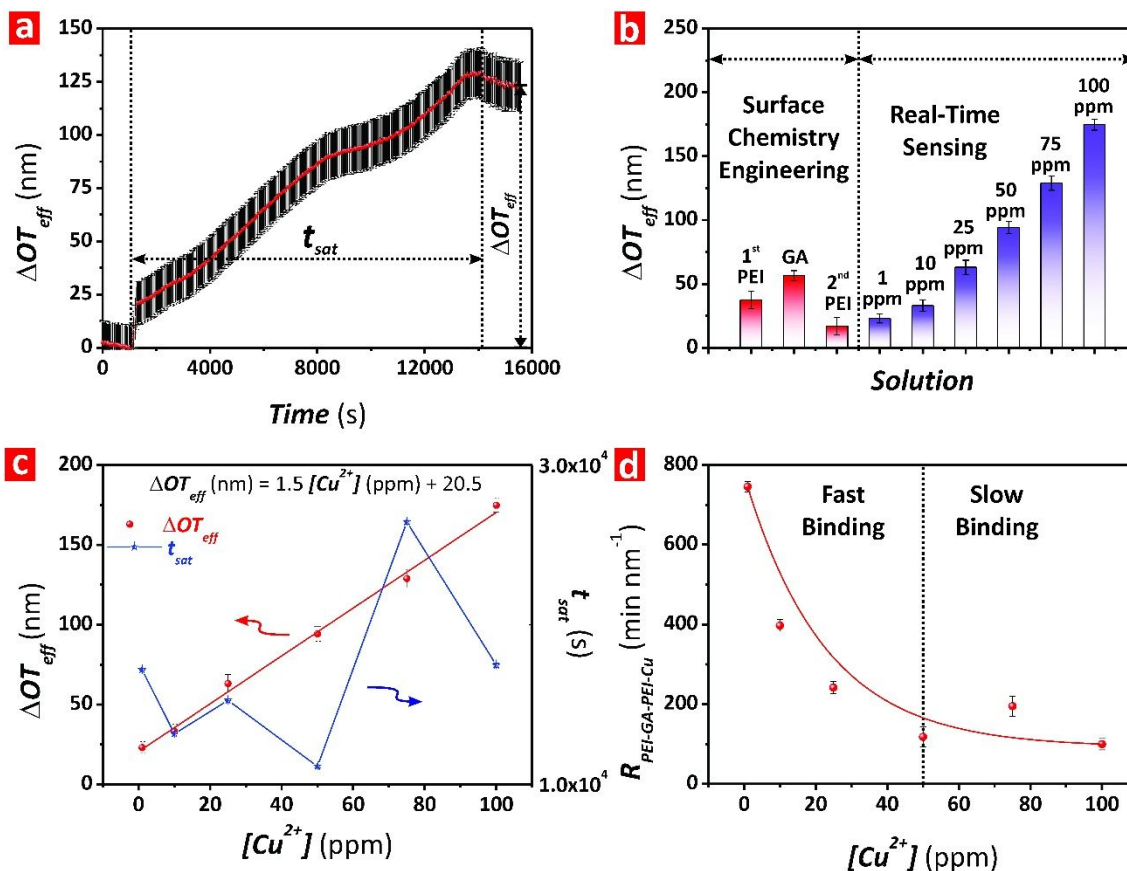


Figure 4. Assessment of the binding interaction between Cu^{2+} ions and PEI-GA-PEI-functionalized NAA interferometers for different concentrations of Cu^{2+} ions (note: error bars denote standard deviation from average measurements obtained from $n = 3$ independent experiments). a) Real-time Cu^{2+} binding stage for $[\text{Cu}^{2+}] = 75$ ppm, where the arrows indicate ΔOT_{eff} and t_{sat} for the binding reaction performed under dynamic flow conditions (note: the dotted line shown at the left of the graph indicates the timepoint at which the Cu^{2+} analytical solution was injected into the flow cell system – OT_{eff} and time baselines). b) Average values of ΔOT_{eff} for each surface chemistry engineering stage and real-time sensing. c) Correlation between ΔOT_{eff} (left scale) and t_{sat} (right scale) with $[\text{Cu}^{2+}]$ for PEI-GA-PEI-functionalized NAA interferometers. d) Kinetic rate ($R_{PEI-GA-PEI-Cu}$) for the binding reaction between Cu^{2+} ions and PEI-GA-PEI functional layers for the range of $[\text{Cu}^{2+}]$ (i.e. 1–100 ppm).

To gain a better insight into the kinetics mechanism of the binding interaction between Cu^{2+} ions and PEI-GA-PEI functional layers, we estimated the binding rate $R_{PEI-GA-PEI-Cu}$, calculated as the ratio between ΔOT_{eff} and t_{sat} for each $[\text{Cu}^{2+}]$ (**Figure 4d**). $R_{PEI-GA-PEI-Cu}$ follows an exponential decay trend with the concentration of copper ions, revealing that, at low concentrations of copper ions (i.e. $[\text{Cu}^{2+}] < 50$ ppm), the increasing concentration of analyte molecules accelerates the

1
2
3 binding reaction due to enhancement of the frequency of interactions between Cu^{2+} ions and the
4 functional groups in the PEI-GA-PEI layer since more ions are available for binding events inside
5 the nanopores. However, for $[\text{Cu}^{2+}] \geq 50$ ppm, the reaction rate becomes almost constant and
6 practically independent on $[\text{Cu}^{2+}]$, indicating that the reaction is rate-limited by the binding affinity
7 between PEI-GA-PEI and Cu^{2+} ions and the conformational changes of PEI molecules upon initial
8 exposure to Cu^{2+} ions.⁵² Note that control experiments with NAA interferometers without PEI-
9 GA-PEI functional layers were performed to verify that red-shifts in the ΔOT_{eff} of PEI-GA-PEI-
10 functionalized NAA interferometers upon exposure to copper ions are exclusively due to selective
11 surface chemistry interactions. Bare NAA interferometers were exposed to 10 and 100 mg L^{-1}
12 analytical solutions of Cu^{2+} ions at pH 5. The measured ΔOT_{eff} for non-modified NAA
13 interferometers upon exposure were ~ 8 and ~ 11 nm, respectively (**Figure S2 – Supporting**
14 **Information**). This result demonstrates that non-specific adsorption of positively charged Cu^{2+}
15 ions to the negatively charged surface of NAA due to electrostatic interactions is almost negligible
16 as compared to ΔOT_{eff} values achieved in PEI-GA-PEI-functionalized NAA interferometers.

36 **3.5. Benchmark Validation of PEI-GA-PEI-Modified NAA Interferometers for Cu^{2+} Sensing.**

37 PEI-GA-PEI-functionalized NAA interferometers were analyzed by XPS after exposure to 1, 25,
38 50 and 100 mg L^{-1} analytical solutions of Cu^{2+} ions. **Figure S3a (Supporting Information)** shows
39 the ratio of copper to nitrogen (Cu/N) established by XPS, demonstrating that, at equilibrium, the
40 amount of copper binding to the chelator (nitrogen) in PEI molecules is linearly dependent on the
41 amount of copper ions present in the analytical solution. Copper binding increases linearly with
42 increasing concentration of Cu^{2+} ions, as indicated by the linear fitting shown in **Figure S3a**. To
43 further validate the selective binding of copper ions, the spatial distribution of Cu in PEI-GA-PEI-
44
45
46
47
48
49
50
51
52
53

1
2
3 modified NAA interferometers was assessed by time-of-flight secondary ion mass spectrometry
4 (ToF-SIMS) and ^{13}C NMR analysis (**Figures S3b and S4 – Supporting Information**).

8 **3.6. Chemical Selectivity of PEI-GA-PEI-Modified NAA Interferometers toward Cu^{2+} Ions.**

9
10 Label-free optical detection systems suffer from non-specific binding interactions, which can lead
11 to false positives or inaccurate quantification of analytes. PEI-GA-PEI-functionalized NAA
12 interferometers were exposed to ion solutions spiked with 25 mg L^{-1} of potentially interfering ions
13 such as Al^{3+} , Fe^{3+} , Cd^{2+} , Ni^{2+} , Pb^{2+} and Zn^{2+} to demonstrate the chemical selectivity toward Cu^{2+}
14 ions. Changes in the effective optical thickness of these films upon exposure to each metal ion
15 solution were compared with those obtained for a 25 mg L^{-1} Cu^{2+} ions solution. All of these
16 analytical solutions were prepared in Milli-Q water with pH adjusted to 5. As **Figure 5a** shows,
17 the ΔOT_{eff} of PEI-GA-PEI-modified NAA interferometers underwent negligible changes upon
18 exposure to Al^{3+} , Fe^{3+} , Ni^{2+} , Pb^{2+} and Zn^{2+} ions. The most significant non-specific change in ΔOT_{eff}
19 was observed for Cd^{2+} (i.e. $0.24 \pm 0.4 \text{ nm}$), which is practically negligible as compared to that
20 measured for the same concentration of Cu^{2+} ions (i.e. $63 \pm 1 \text{ nm}$, ~ 262 times higher). Fourier
21 transform infrared spectroscopy (FTIR) and X-ray absorption spectroscopy (XAS) analyses in our
22 previous study indicate that GA crosslinking of PEI molecules generates structural changes that
23 lead to the formation of a PEI network containing a high content of Schiff bases (i.e. imine
24 nitrogens), with strong affinity and selectivity toward copper ions.³⁸ These results demonstrate that
25 PEI-GA-PEI-functionalized NAA interferometers feature high sensitivity and selectivity toward
26 Cu^{2+} ions due to their functional surface chemistry architecture.

51 **3.7. Real-Life Application of PEI-GA-PEI-Modified NAA Interferometers for Cu^{2+} Ions**

52 **Sensing.** PEI-GA-PEI-functionalized NAA interferometers were exposed to complex, real acid
53 mine drainage liquid (AMD) and tap water spiked with Cu^{2+} ions for detection and quantification
54
55
56
57

1
2
3 of copper ions in complex matrices (**Figure 5**). **Table S1 (Supporting Information)** shows the
4 concentration of dissolved metals present in the AMD solution analyzed in our study. Analysis of
5 the AMD solution by ICP-OES revealed that Al ($\sim 130 \text{ mg L}^{-1}$) and Fe ($> 500 \text{ mg L}^{-1}$) were the
6 most abundant metal ions in these samples, with more than four-fold and sixteen-fold higher
7 concentrations, respectively, than other metal ions such as copper ($\sim 31 \text{ mg L}^{-1}$) and zinc ($\sim 20 \text{ mg}$
8 L^{-1}). Freshly prepared PEI-GA-PEI-functionalized NAA interferometers were exposed to the
9 AMD solution and changes in the effective optical thickness were assessed in real-time by RIfS
10 (**Figure 5b**). The PEI-GA-PEI surface chemistry on the inner surface of NAA interferometers was
11 engineered following the protocol outlined in Section 3.3. After the final functionalization step,
12 Milli Q-water at pH 5 was flowed through the system for 15 min to obtain a stable baseline. Then,
13 the AMD analyte solution was flowed through the flow cell system. The ΔOT_{eff} of PEI-GA-PEI-
14 functionalized NAA interferometers increased sharply as a result of Cu^{2+} ions binding. Once the
15 equilibrium was achieved (i.e. plateau in ΔOT_{eff}), Milli-Q water (pH 5) was flowed again through
16 the system to establish the total ΔOT_{eff} resulting from the selective binding of Cu^{2+} ions present in
17 the AMD solution. This protocol was repeated to analyze the system's performance using tap water
18 spiked with 25 mg L^{-1} of Cu^{2+} ions. Real-time monitoring of these binding processes through
19 ΔOT_{eff} is shown in **Figure 5b**. The RIfS response in terms of ΔOT_{eff} for these processes established
20 values of $69 \pm 1 \text{ nm}$ and $70 \pm 2 \text{ nm}$ for AMD and tap water solutions, respectively (**Figure 5c**).
21 Using the calibration line obtained in **Figure 4c**, such a change in effective optical thickness
22 corresponds to a concentration of copper ions of $32 \pm 1 \text{ mg L}^{-1}$. Interestingly, the amount of copper
23 quantified using ICP-OES from the same AMD analyte solution was $\sim 30.8 \text{ mg L}^{-1}$, which would
24 correspond to a total ΔOT_{eff} of $\sim 66.7 \text{ nm}$.

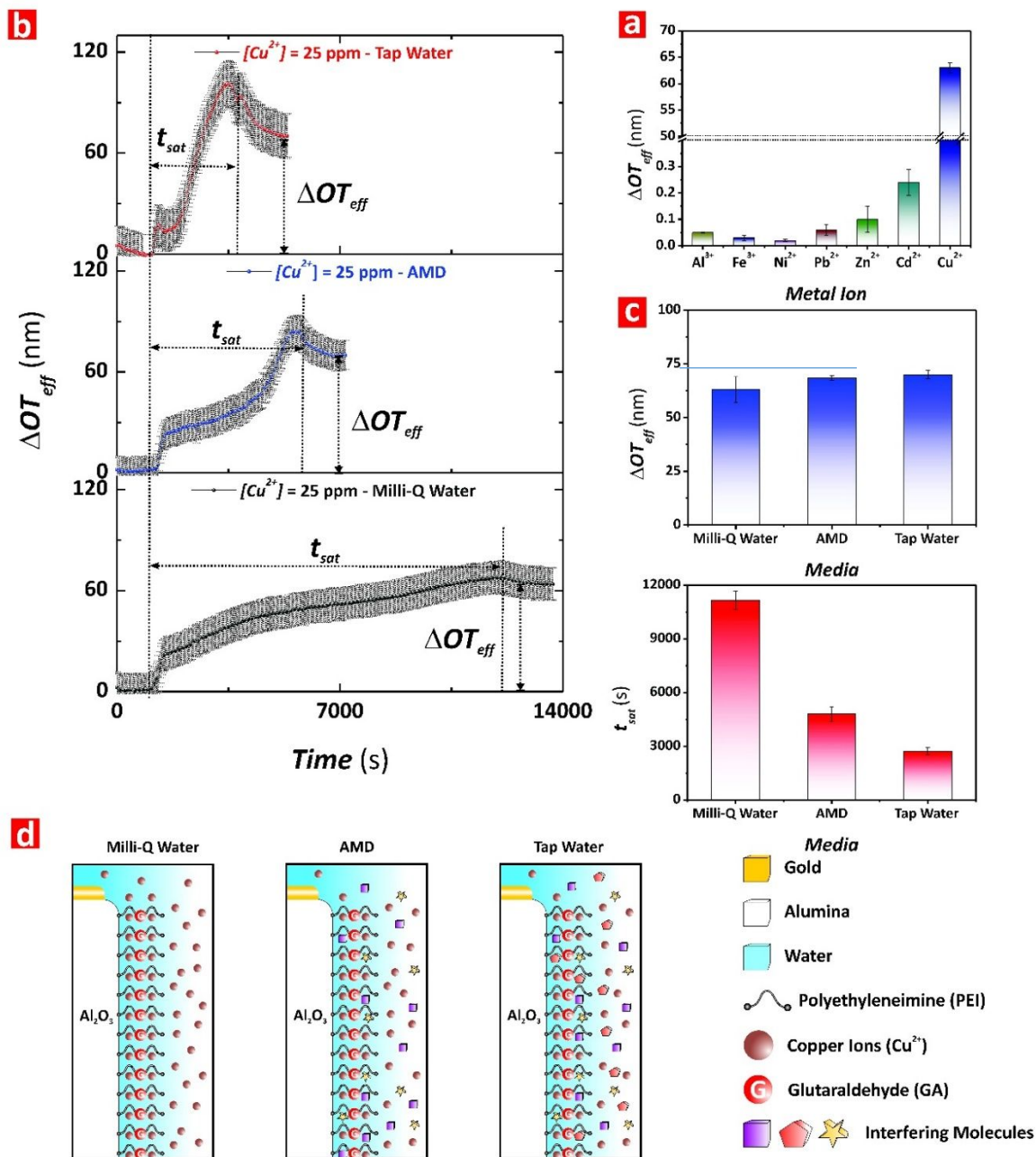


Figure 5. Assessment of chemical selectivity of PEI-GA-PEI-functionalized NAA interferometers for Cu²⁺ ions and performance assessment in complex matrices (note: error bars denote standard deviation from average measurements obtained from n = 3 independent experiments). a) Bar chart showing the ΔOT_{eff} measured upon exposure to analytical solutions of Al³⁺, Fe³⁺, Cd²⁺, Ni²⁺, Pb²⁺, Zn²⁺ and Cu²⁺ (i.e. [metal ion] = 25 ppm). b) Real-time Cu²⁺ binding stage for each media (i.e. Milli-Q water, AMD and tap water for [Cu²⁺] = 25 ppm), where the arrows indicate ΔOT_{eff} and t_{sat} for each of these binding reactions performed under dynamic flow conditions (note: the dotted line shown at the left of the graphs indicates the timepoint at which the analytical solutions were injected into the flow cell system – OT_{eff} and time baselines). c) Bar chart showing the ΔOT_{eff} (top) and t_{sat} (bottom) measured in PEI-GA-PEI-functionalized NAA interferometers upon exposure to analytical and real-life

1
2
3 solutions of Cu^{2+} (i.e. $[\text{Cu}^{2+}] = 25$ ppm). d) Schematic representation illustrating the effect of the media complexity
4 (i.e. interfering molecules) on the sensing performance of PEI-GA-PEI-modified NAA interferometers.
5

6
7 Therefore, the sensing performance of our RIfS system only deviates $\sim 4.5\%$ from the
8 concentration value provided by a benchmark technique such as ICP-OES. This system could
9 provide a cost-competitive solution for in-situ copper ions sensing at a significantly reduced price
10 per analysis, with miniaturized features for portability. The saturation time (t_{sat}) for the binding
11 reaction between Cu^{2+} and PEI-GA-PEI functional layers decreases in the following order Milli-
12 Q water (11152 ± 450 s) > AMD (4797 ± 350 s) > tap water (2716 ± 200 s). The higher response
13 of our RIfS system in terms of ΔOT_{eff} for the AMD and tap water solutions can be attributed to the
14 ionic strength of the solution. We speculate that the presence of other interfering organic and
15 inorganic ions and complexes in these matrices modifies the ionic strength of the medium. This
16 could influence the conformation of PEI functional molecules so more binding groups are exposed
17 to copper ions in the nanopores, increasing the binding reaction rate and reducing the saturation
18 time of the reaction (**Figure 5d**). The excellent agreement between the results obtained by RIfS
19 and ICP-OES for the quantification of copper ions clearly demonstrates the suitability of our
20 sensing system to detect copper ions in real-life environmental samples.
21
22
23
24
25
26
27
28
29
30
31
32
33
34
35
36
37
38

39 CONCLUSIONS

40
41
42 In summary, this study has demonstrated the development of a label-free, real-time sensing
43 system for the detection and quantification of copper ions combining nanoporous anodic alumina
44 interferometers functionalized with double-layered glutaraldehyde-crosslinked polyethyleneimine
45 and reflectometric interference spectroscopy. The sensing performance parameters were
46 established using analytical solutions of Cu^{2+} ions, where changes in the effective optical thickness
47 of PEI-GA-PEI-functionalized NAA interferometers upon exposure to Cu^{2+} ions were used as
48 sensing principle. The linear detection range of this system spans from 1 to 100 mg L^{-1} , with a
49
50
51
52
53
54
55
56
57
58
59
60

1
2
3 sensitivity of $1.5 \pm 0.1 \text{ nm (mg L}^{-1}\text{)}^{-1}$, a low limit of detection of $0.007 \pm 0.001 \text{ mg L}^{-1}$ and a
4
5 linearity of 0.9926. The chemical selectivity of the sensing system was assessed by exposing PEI-
6
7 GA-PEI-modified NAA platforms to analytical solutions containing controlled amounts of
8
9 potentially interfering ions such as Fe^{3+} , Cd^{2+} , Al^{3+} , Ni^{2+} , Pb^{2+} and Zn^{2+} . The surface chemistry of
10
11 the system showed excellent selectivity toward Cu^{2+} ions and the effective optical thickness
12
13 changes associated with other interfering ions were negligible as compared to those obtained for
14
15 Cu^{2+} ions. Finally, we evaluated the performance of the system for real-life applications,
16
17 establishing concentration of copper ions present in real acid mine drainage liquid and spiked tap
18
19 water. The obtained results only deviated $\sim 4.5\%$ from the value obtained using ICP-OES.
20
21
22
23

24 Notes

25
26 The authors declare no competing financial interest.
27

28 ACKNOWLEDGEMENTS

29
30
31 Authors thank the support provided by the Australian Research Council (ARC) through the grants
32
33 number DE140100549 and CE140100003, the School of Chemical Engineering, the University of
34
35 Adelaide (UoA), the Institute for Photonics and Advanced Sensing (IPAS), the ARC Centre of
36
37 Excellence for Nanoscale BioPhotonics (CNBP), the National Health and Medical Research
38
39 Council (NHMRC) through grant numbers GNT1143296 and GNT1146627, and The University
40
41 of Queensland.
42

43 ASSOCIATED CONTENT

44
45 **Supporting Information.** The Supporting Information file provides further details on the optical
46
47 set-up, ^{13}C NMR spectra of PEI molecules, XPS and ToF-SIMS analyses, real-time monitoring of
48
49 ΔOT_{eff} for different concentrations of copper ions, control experiments in as-produced NAA
50
51 interferometers without PEI-GA-PEI functional layers, and a table summarizing the metal
52
53 concentration in acid mine drainage liquid by ICP-OES. This material is available free of charge
54
55 via the Internet at <http://pubs.acs.org>.
56
57
58
59
60

REFERENCES

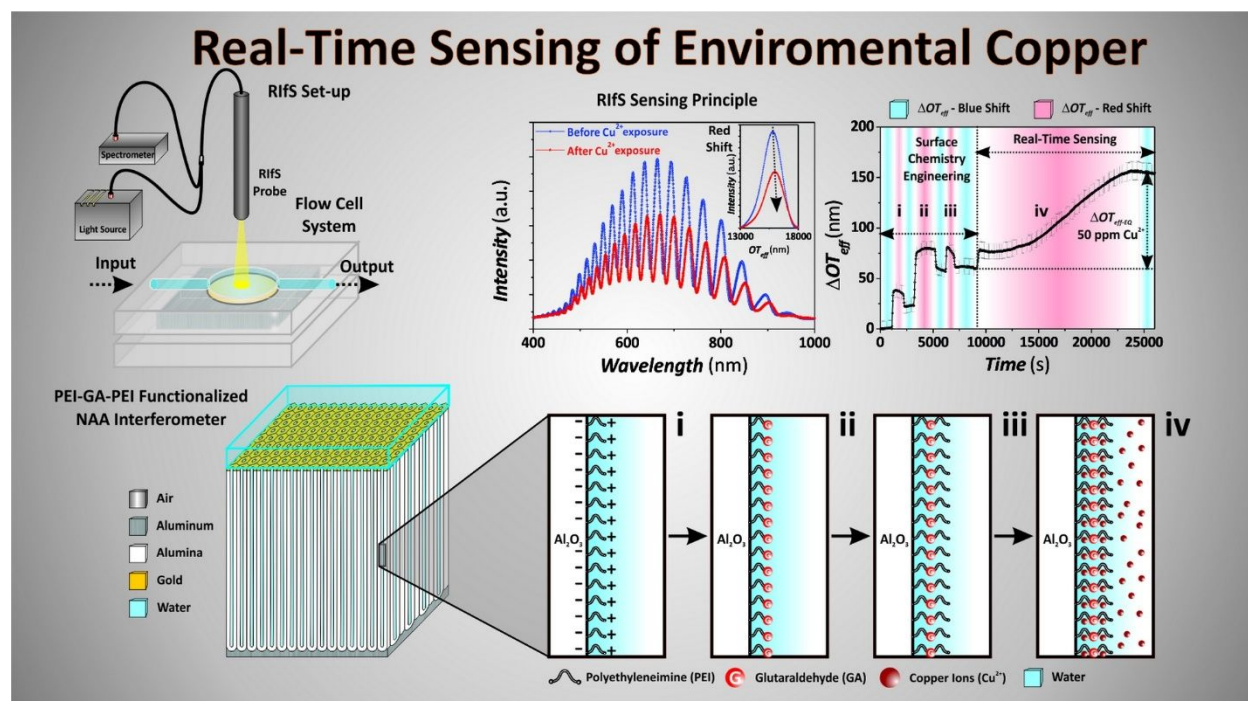
1. Husein, H. e. H.; Fernandez, C. R., Cosmeceuticals: Peptides, Proteins, and Growth Factors. *Journal of Cosmetic Dermatology* **2016**, *15* (4), 514-519.
2. Rai, M.; Ingle, A., Role of Nanotechnology in Agriculture with Special Reference to Management of Insect Pests. *Appl. Microbiol. Biotechnol.* **2012**, *94* (2), 287-293.
3. Van Beers, D.; Graedel, T., The Magnitude and Spatial Distribution of In-Use Copper Stocks in Cape Town, South Africa. *S. Afr. J. Sci.* **2003**, *99* (1-2), 61-69.
4. Richardson, H. W., *Handbook of Copper Compounds and Applications*. CRC Press: **1997**.
5. Pagett, R., Energy and Commodities. In *Building Global Resilience in the Aftermath of Sustainable Development: Planet, People and Politics*, Springer International Publishing: Cham, **2018**, pp 83-86.
6. Claisse, D.; Alzieu, C., Copper Contamination as a Result of Antifouling Paint Regulations? *Mar. Pollut. Bull.* **1993**, *26* (7), 395-397.
7. Castritsi-Catharios, J.; Neofitou, N.; Vorloou, A., Comparison of Heavy Metal Concentrations in Fish Samples from Three Fish Farms (Eastern Mediterranean) Utilizing Antifouling Paints. *Toxicol. Environ. Chem.* **2015**, *97* (1), 116-123.
8. Chung, B. Y.; Song, C. H.; Park, B. J.; Cho, J. Y., Heavy Metals in Brown Rice (*Oryza sativa* L.) and Soil After Long-Term Irrigation of Wastewater Discharged from Domestic Sewage Treatment Plants. *Pedosphere* **2011**, *21* (5), 621-627.
9. Gunatilake, S., Methods of Removing Heavy Metals from Industrial Wastewater. *Methods* **2015**, *1* (1).
10. Samsudeen, N.; Matheswaran, M., Bioremediation of Industrial Wastewater Using Bioelectrochemical Treatment. In *Bioremediation: Applications for Environmental Protection and Management*, Springer: **2018**, pp 115-126.
11. Cao, Z. H.; Hu, Z. Y., Copper Contamination in Paddy Soils Irrigated with Wastewater. *Chemosphere* **2000**, *41* (1), 3-6.
12. Minkina, T. M.; Linnik, V. G.; Nevidomskaya, D. G.; Bauer, T. V.; Mandzhieva, S. S.; Khoroshavin, V. Y., Forms of Cu (II), Zn (II), and Pb (II) Compounds in Technogenically Transformed Soils Adjacent to the Karabashmed Copper Smelter. *J. Soils Sediments* **2018**, *6* (18), 2217-2228.
13. Kaur, S.; Kempson, I.; Xu, H.; Nydén, M.; Larsson, M., Bio-Template Assisted Synthesis of Porous Glutaraldehyde-Polyethyleneimine Particulate Resin for Selective Copper Ion Binding and Recovery. *RSC Adv.* **2018**, *8* (22), 12043-12052.
14. Flemming, C.; Trevors, J., Copper Toxicity and Chemistry in the Environment: a review. *Water, Air, Soil Pollut.* **1989**, *44* (1-2), 143-158.

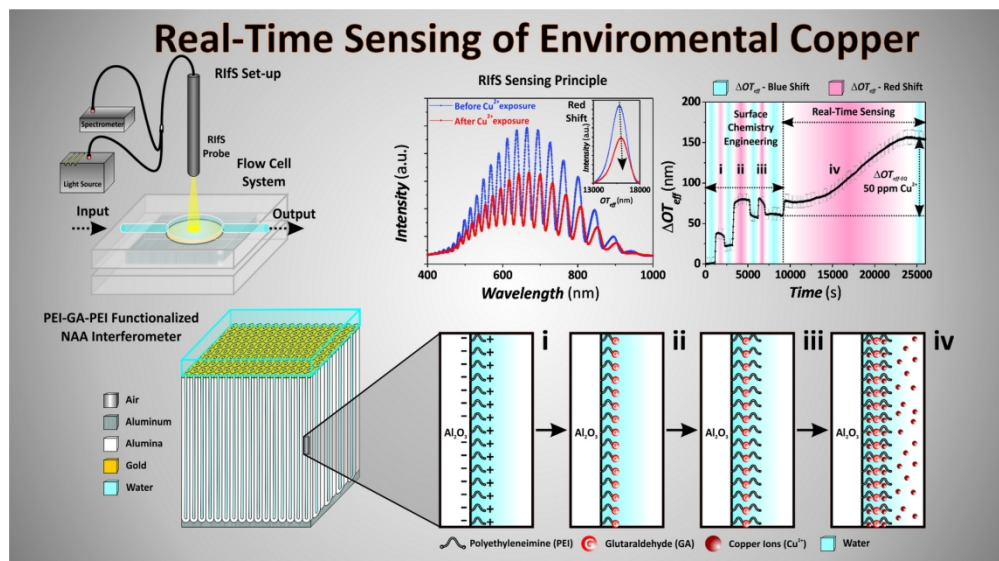
- 1
2
3 15. Al-Saydeh, S. A.; El-Naas, M. H.; Zaidi, S. J., Copper Removal From Industrial Wastewater: A Comprehensive Review. *J. Ind. Eng. Chem.* **2017**, *56*, 35-44.
- 4
5
6 16. Cui, C.; He, M.; Hu, B., Membrane Solid Phase Microextraction with Alumina Hollow Fiber
7 on Line Coupled with ICP-OES for the Determination of Trace Copper, Manganese and Nickel in
8 Environmental Water Samples. *J. Hazard. Mater.* **2011**, *187* (1-3), 379-385.
- 9
10 17. Freedman, Y. E.; Ronen, D.; Long, G. L., Determination of Cu and Cd Content of Groundwater
11 Colloids by Solid Sampling Graphite Furnace Atomic Absorption Spectrometry. *Environ. Sci.*
12 *Technol.* **1996**, *30* (7), 2270-2277.
- 13
14 18. Nolan, M. A.; Kounaves, S. P., Microfabricated Array of Iridium Microdisks as a Substrate for
15 Direct Determination of Cu²⁺ or Hg²⁺ Using Square-Wave Anodic Stripping Voltammetry. *Anal.*
16 *Chem.* **1999**, *71* (16), 3567-3573.
- 17
18 19. Wen, T.; Qu, F.; Li, N. B.; Luo, H. Q., A Facile, Sensitive, and Rapid Spectrophotometric
19 Method for Copper (II) Ion Detection in Aqueous Media Using Polyethyleneimine. *Arabian J.*
20 *Chem.* **2017**, *10*, S1680-S1685.
- 21
22 20. Eckstein, C.; Acosta, L. K.; Pol, L.; Xifré-Pérez, E.; Pallares, J.; Ferré-Borrull, J.; Marsal, L.
23 F. Nanoporous Anodic Alumina Surface Modification by Electrostatic, Covalent, and Immune
24 Complexation Binding Investigated by Capillary Filling. *ACS Appl. Mater. Interfaces* **2018**, *10*
25 (12), 10571-10579.
- 26
27 21. Mariani, S.; Strambini, L. M.; Barillaro, G. Femtomole Detection of Proteins Using a Label-
28 Free Nanostructured Porous Silicon Interferometer for Perspective Ultrasensitive Biosensing. *Anal*
29 *Chem.* **2016** *88* (17), 8502-8509.
- 30
31 22. Möhrle, B. P.; Köhler, K.; Jaehrling, J.; Brock, R.; Gauglitz, G., Label-Free Characterization
32 of Cell Adhesion Using Reflectometric Interference Spectroscopy (RIFS). *Anal. Bioanal. Chem.*
33 **2006**, *384* (2), 407-413.
- 34
35 23. Gauglitz, G.; Brecht, A.; Kraus, G.; Mahm, W., Chemical and Biochemical Sensors Based on
36 Interferometry at Thin (Multi-) Layers. *Sens. Actuators, B* **1993**, *11* (1-3), 21-27.
- 37
38 24. Curtis, C. L.; Doan, V. V.; Credo, G. M.; Sailor, M. J., Observation of Optical Cavity Modes
39 in Photoluminescent Porous Silicon Films. *J. Electrochem. Soc.* **1993**, *140* (12), 3492-3494.
- 40
41 25. Belge, G.; Beyerlein, D.; Betsch, C.; Eichhorn, K.-J.; Gauglitz, G.; Grundke, K.; Voit, B.,
42 Suitability of Hyperbranched Polyester for Sensoric Applications—Investigation with
43 Reflectometric Interference Spectroscopy. *Anal. Bioanal. Chem.* **2002**, *374* (3), 403-411.
- 44
45 26. Santos, A.; Kumeria, T.; Losic, D., Optically Optimized Photoluminescent and Interferometric
46 Biosensors Based on Nanoporous Anodic Alumina: A Comparison. *Anal. Chem.* **2013**, *85* (16),
47 7904-7911.
- 48
49 27. Kumeria, T.; Rahman, M. M.; Santos, A.; Ferré-Borrull, J.; Marsal, L. F.; Losic, D., Structural
50 and Optical Nanoengineering of Nanoporous Anodic Alumina Rugate Filters for Real-Time and
51 Label-Free Biosensing Applications. *Anal. Chem.* **2014**, *86* (3), 1837-1844.
- 52
53
54
55
56
57
58
59
60

- 1
2
3 28. Mariani, S.; Robbiano, V.; Strambini, L.M.; Debrassi, A.; Egri, G.; Dähne, L.; Barillaro, G.,
4 Layer-by-Layer Biofunctionalization of Nanostructured Porous Silicon for High-Sensitivity and
5 High-Selectivity Label-Free Affinity Biosensing. *Nat. Comm.* **2018**, *9*, 5256.
6
7 29. Kacmaz, S.; Ertekin, K.; Mercan, D.; Oter, O.; Cetinkaya, E.; Celik, E., An Ultra Sensitive
8 Fluorescent Nanosensor for Detection of Ionic Copper. *Spectrochim. Acta, Part A* **2015**, *135*, 551-
9 559.
10
11 30. Choi, H. W.; Sakata, Y.; Kurihara, Y.; Ooya, T.; Takeuchi, T., Label-Free Detection of C-
12 Reactive Protein Using Reflectometric Interference Spectroscopy-Based Sensing System. *Anal.*
13 *Chim. Acta* **2012**, *728*, 64-68.
14
15 31. Piehler, J.; Brecht, A.; Gauglitz, G., Affinity Detection of Low Molecular Weight Analytes.
16 *Anal. Chem.* **1996**, *68* (1), 139-143.
17
18 32. Chen, Y.; Santos, A.; Wang, Y.; Kumeria, T.; Wang, C.; Li, J.; Losic, D., Interferometric
19 Nanoporous Anodic Alumina Photonic Coatings for Optical Sensing. *Nanoscale* **2015**, *7* (17),
20 7770-7779.
21
22 33. Lin, V. S.-Y.; Motesharei, K.; Dancil, K.-P. S.; Sailor, M. J.; Ghadiri, M. R., A Porous Silicon-
23 Based Optical Interferometric Biosensor. *Science* **1997**, *278* (5339), 840-843.
24
25 34. Sauer, M.; Brecht, A.; Charissé, K.; Maier, M.; Gerster, M.; Stemmler, I.; Gauglitz, G.; Bayer,
26 E., Interaction of Chemically Modified Antisense Oligonucleotides with Sense DNA: A Label-
27 Free Interaction Study with Reflectometric Interference Spectroscopy. *Anal. Chem.* **1999**, *71* (14),
28 2850-2857.
29
30 35. Kumeria, T.; Kurkuri, M. D.; Diener, K. R.; Parkinson, L.; Losic, D., Label-Free
31 Reflectometric Interference Microchip Biosensor Based on Nanoporous Alumina for Detection of
32 Circulating Tumour Cells. *Biosens. Bioelectron.* **2012**, *35* (1), 167-173.
33
34 36. Santos, A.; Balderrama, V. S.; Alba, M.; Formentín, P.; Ferré-Borrull, J.; Pallarès, J.; Marsal,
35 L. F., Nanoporous Anodic Alumina Barcodes: Toward Smart Optical Biosensors. *Adv. Mater.*
36 **2012**, *24* (8), 1050-1054.
37
38 37. Lindén, J. B.; Larsson, M.; Coad, B. R.; Skinner, W. M.; Nydén, M., Polyethyleneimine for
39 Copper Absorption: Kinetics, Selectivity and Efficiency in Artificial Seawater. *RSC Adv.* **2014**, *4*
40 (48), 25063-25066.
41
42 38. Lindén, J. B.; Larsson, M.; Kaur, S.; Skinner, W. M.; Miklavcic, S. J.; Nann, T.; Kempson, I.
43 M.; Nydén, M., Polyethyleneimine for Copper Absorption II: Kinetics, Selectivity and Efficiency
44 from Seawater. *RSC Adv.* **2015**, *5* (64), 51883-51890.
45
46 39. Masuda, H.; Fukuda, K., Ordered Metal Nanohole Arrays Made by a Two-Step Replication of
47 Honeycomb Structures of Anodic Alumina. *Science* **1995**, *268* (5216), 1466-1468.
48
49 40. Nielsch, K.; Choi, J.; Schwirn, K.; Wehrspohn, R. B.; Gösele, U., Self-Ordering Regimes of
50 Porous Alumina: the 10 Porosity Rule. *Nano Lett.* **2002**, *2* (7), 677-680.
51
52 41. Lee, W.; Park, S.-J., Porous Anodic Aluminum Oxide: Anodization and Templated Synthesis
53 of Functional Nanostructures. *Chem. Rev.* **2014**, *114* (15), 7487-7556.
54
55
56
57
58
59
60

- 1
2
3 42. Santos, A.; Kumeria, T.; Losic, D., Nanoporous Anodic Aluminum Oxide for Chemical
4 Sensing and Biosensors. *TrAC, Trends Anal. Chem.* **2013**, *44*, 25-38.
5
6 43. Macias, G.; Hernández-Eguía, L. P.; Ferré-Borrull, J.; Pallares, J.; Marsal, L. F. Gold-Coated
7 Ordered Nanoporous Anodic Alumina Bilayers for Future Label-Free Interferometric Biosensors.
8 *ACS Appl. Mater. Interfaces* **2013**, *5* (16), 8093-8098.
9
10 44. Kumeria, T.; Losic, D., Controlling Interferometric Properties of Nanoporous Anodic
11 Aluminium Oxide. *Nanoscale Res. Lett.* **2012**, *7* (1), 88.
12
13 45. Dronov, R.; Jane, A.; Shapter, J. G.; Hodges, A.; Voelcker, N. H., Nanoporous Alumina-Based
14 Interferometric Transducers Ennobled. *Nanoscale* **2011**, *3* (8), 3109-3114.
15
16 46. Law, C. S.; Sylvia, G. M.; Nemati, M.; Yu, J.; Losic, D.; Abell, A. D.; Santos, A. Engineering
17 of Surface Chemistry for Enhanced Sensitivity in Nanoporous Interferometric Sensing Platforms.
18 *ACS Appl. Mater. Interfaces* **2017**, *9* (10), 8929-8940.
19
20 47. Kumeria, T.; Gulati, K.; Santos, A.; Losic, D. Real-time and in Situ Drug Release Monitoring
21 from Nanoporous Implants under Dynamic Flow Conditions by Reflectometric Interference
22 Spectroscopy. *ACS Appl. Mater. Interfaces* **2013**, *5* (12), 5436-5442.
23
24 48. Lindén, J. B.; Larsson, M.; Kaur, S.; Nosrati, A.; Nydén, M., Glutaraldehyde-Crosslinking for
25 Improved Copper Absorption Selectivity and Chemical Stability of Polyethyleneimine Coatings.
26 *J. Appl. Polym. Sci.* **2016**, 43954.
27
28 49. Kaur, S.; Kempson, I. M.; Lindén, J. B.; Larsson, M.; Nydén, M., Unhindered Copper Uptake
29 by Glutaraldehyde-Polyethyleneimine Coatings in an Artificial Seawater Model System with
30 Adsorbed Swollen Polysaccharides and Competing Ligand EDTA. *Biofouling* **2017**, *33* (2), 184-
31 194.
32
33 50. Kumeria, T.; Rahman, M. M.; Santos, A.; Ferré-Borrull, J.; Marsal, L. F.; Losic, D.,
34 Nanoporous Anodic Alumina Rugate Filters for Sensing of Ionic Mercury: Toward Environmental
35 Point-of-Analysis Systems. *ACS Appl. Mater. Interfaces* **2014**, *6* (15), 12971-12978.
36
37 51. Maketon, W.; Zenner, C. Z.; Ogden, K. L. Removal Efficiency and Binding Mechanisms of
38 Copper and Copper-EDTA Complexes Using Polyethyleneimine. *Environ. Sci. Technol.* **2008**, *42*
39 (6), 2124-2129.
40
41 52. Law, C. S.; Lim, S. Y.; Abell, A. D.; Santos, A. Real-Time Binding Monitoring between
42 Human Blood Proteins and Heavy Metal Ions in Nanoporous Anodic Alumina Photonic Crystals.
43 *Anal. Chem.* **2018**, *90* (16), 10039-10048.
44
45
46
47
48
49
50
51
52
53
54
55
56
57
58
59
60

TABLE OF CONTENTS





for TOC only

705x394mm (72 x 72 DPI)